CHEMISTRY
A EUROPEAN JOURNAL

DOI: 10.1002/chem.200501450

Experimental and Theoretical Investigations of the Sulfite-Based Polyoxometalate Cluster Redox Series: α- and β-$[Mo_{18}O_{54}(SO_3)_2]^{4-/5-/6-}$

Carole Baffert,[a] John F. Boas,[b] Alan M. Bond,*[a] Paul Kögerler,[c] De-Liang Long,[d] John R. Pilbrow,[b] and Leroy Cronin*[d]

Abstract: The synthesis, isolation and structural characterization of the sulfite polyoxomolybdate clusters α-(D_{3h})-$(C_{20}H_{44}N)_4\{\alpha\text{-}[Mo_{18}O_{54}(SO_3)_2]\}\cdot CH_3CN$ and β-(D_{3d})$(C_{20}H_{44}N)_4\{\beta\text{-}[Mo_{18}O_{54}(SO_3)_2]\}\cdot CH_3CN$ is presented. Voltammetric studies in acetonitrile (0.1 M Hx_4NClO_4, Hx_4N = tetra-*n*-hexylammonium) reveal the presence of an extensive series of six one-electron reduction processes for both isomers. Under conditions of bulk electrolysis, the initial $[Mo_{18}O_{54}(SO_3)_2]^{4-/5-}$ and $[Mo_{18}O_{54}(SO_3)_2]^{5-/6-}$ processes produce stable $[Mo_{18}O_{54}(SO_3)_2]^{5-}$ and $[Mo_{18}O_{54}(SO_3)_2]^{6-}$ species, respectively, and the same reduced species may be produced by photochemical reduction. Spectroelectrochemical data imply that retention of structural form results upon reduction, so that both α and β isomers are available at each of the 4-, 5-, and 6-redox levels. However, the α isomer is the thermodynamically favored species in both the one- and two-electron-reduced states, with β→α isomerization being detected in both cases on long time scales (days). EPR spectra also imply that increasing localization of the unpaired electron occurs over the α- and β-$[Mo_{18}O_{54}(SO_3)_2]^{5-}$ frameworks as the temperature approaches 2 K where the EPR spectra show orthorhombic symmetry with different *g* and hyperfine values for the α and β isomers. Theoretical studies support the observation that it is easier to reduce the α cluster than the β form and also provide insight into the driving force for β→α isomerization in the reduced state. Data are compared with that obtained for the well studied α-$[Mo_{18}O_{54}(SO_4)_2)]^{4-}$ sulfate cluster.

Keywords: density functional calculations · electrochemistry · EPR spectroscopy · molybdenum · polyoxometalates · sulfite

Introduction

Polyoxometalates (POMs) constitute a class of inorganic cluster compounds that are of eminent interest due to their vastly diverse structures[1] and properties.[2] Both iso- and heteropolyoxometalates have been studied intensively to elucidate their electronic and molecular properties that give rise to a variety of applications in catalysis,[3–5] medicinal chemistry[6–8] and materials science.[9–14] One particular characteristic of POMs is the formation of thermodynamically very stable and high symmetric structural archetypes, such as the O_h-symmetric $\{M_6\}$ Lindqvist, the T_d-symmetric $\{M_{12}\}$ Keggin, and the D_{3h}-symmetric $\{M_{18}\}$ Dawson anions.

The Dawson structural type ($[M_{18}O_{54}(XO_4)_2]^{m-}$; M = Mo, W, and X = P, S), which is of interest in this paper, was discovered over fifty years ago and since then has been the subject of hundreds of papers.[15,16] The conventional Dawson structure incorporates two tetrahedral anions such as PO_4^{3-},[15,16] AsO_4^{3-},[17] SO_4^{2-},[18–20] or ClO_4^-[21,22] within the elongated polyoxometalate cluster shell. In contrast only a few examples of $\{M_{18}\}$ Dawson-like cluster hosts that contain non-tetrahedral anions are available. Examples include a single pyramidal anion (BiO_3^{3-} or AsO_3^{3-}) in each cluster,[23,24] or a di-tetrahedral anion ($P_2O_7^{4-}$, containing two corner-sharing tetrahedra).[25–28] We recently synthesized

[a] Dr. C. Baffert, Prof. A. M. Bond
School of Chemistry, Monash University
Clayton, Victoria 3800 (Australia)
E-mail: alan.bond@sci.monash.edu.au

[b] Dr. J. F. Boas, Prof. J. R. Pilbrow
School of Physics, Monash University
Clayton, Victoria 3800 (Australia)

[c] Dr. P. Kögerler
Ames Laboratory and Department of Physics & Astronomy
Iowa State University
Ames, IA 50011 (USA)

[d] Dr. D.-L. Long, Prof. L. Cronin
Department of Chemistry
The University of Glasgow
Glasgow, G12 8QQ (UK)
E-mail: L.Cronin@chem.gla.ac.uk

Supporting information for this article is available on the WWW under http://www.chemeurj.org/ or from the author.

clusters with a metal–oxo framework that resembles the Dawson structure, but incorporates two pyramidal anions[29] rather than the tetrahedral anions found in the Wells–Dawson structure type. This endeavor was motivated by the fact that such clusters containing pyramidal anions may exhibit novel properties arising from the intramolecular electronic interactions between the two closely grouped anions that are ligated to the two $\{M_9\}$ halves of the cluster sphere. We selected sulfite (SO_3^{2-}) as a prototypal pyramidal anion for our studies, as it matches the size requirements of the M_{18} cluster sphere and represents a relatively polarizable, soft Lewis base. Furthermore, structurally characterized polyoxomolybdosulfites of this kind are rare. Examples include $(NH_4)_4[Mo_5O_{15}(SO_3)_2]\cdot 4H_2O$,[30] $(NH_4)_8[Mo_2O_4(SO_3)_2]\cdot 2H_2O$[31] and the framework structures $(NH_4)_{20}[Mo_{12}O_{24}(SO_3)_{16}]\cdot 4H_2O$[31] and $(NH_4)_{15}\{Na[Mo_{12}O_{24}(SO_3)_4]_2\}\cdot 5H_2O$.[31] These structures are of potential biological interest as one kind of sulfite oxidase is based on molybdenum metalloenzymes. In this context, the structural and electronic characterization of POM-based sulfite is an attractive goal.[32–34]

In our previous work, an unprecedented class of 18-molybdosulfite clusters, $[Mo_{18}O_{54}(SO_3)_2]^{4-}$ was isolated and characterized in two isomeric forms.[29] In both configurations, the pyramidal, C_{3v}-symmetric SO_3 groups are aligned with the principal C_3 axis of the cluster, whereby the lone electron pairs are oriented toward each other within the cluster shell and the S–S distances of 3.23 and 3.27 Å fall below the sum of sulfur van der Waals radii of 3.6 Å. These α and β isomers differ in their relative orientation of the two SO_3 moieties and their adjoined $\{Mo_9\}$ cluster halves, whereby the two $\{SMo_9\}$ half units are either mirrored (α) or rotated by 60° to each other (β) (Figure 1). Both isomers were found to exhibit fully reversible thermochromism and their tetrabutylammonium salts change color from pale green at 77 K to dark red at 500 K. This fact is attributed to a pronounced dependency of the lowest unoccupied molecular orbitals on small geometrical changes of the oxo positions of the polyoxomolybdate framework that are typical for thermal vibrations, while the two highest occupied molecular orbitals, centered on the sulfite groups, remain energetically unaffected by these vibrations.[23]

Intuitively, it may be envisaged that direct comparison of isomers of the sulfite and the well-known $[M_{18}O_{54}(SO_4)_2]^{4-}$ Wells–Dawson anions should be possible. However, it is important to note subtle nomenclature differences used to describe the two sets of cluster may need to be considered. Many isomers are possible for the classical Wells–Dawson sulfate structure with tetrahedral anions and these are referred to as α, β, γ, α*, β*, and γ*.[35] In contrast, there are only two possible isomers for $[Mo_{18}O_{54}(SO_3)_2]^{4-}$ clusters that have been labeled α and β. Although both the α-sulfite $\{Mo_{18}\}$ cluster and the alpha Wells–Dawson sulfate cluster have comparable metal–oxo frameworks with D_{3h} symmetry, the β-sulfite $\{Mo_{18}\}$ has a metal–oxo framework that has D_{3d} symmetry. Thus, whilst the two β forms can be said to be related with respect to relative positions of the capping Mo atoms (Figure 1), in terms of symmetry the D_{3d} γ*-Wells–Dawson cluster and not the β-Wells–Dawson may have more comparable metal–oxo framework structures.[35] For purposes of comparison, only the α form of $[Mo_{18}O_{54}(SO_4)_2]^{4-}$ has been characterized[36] but there is a D_{3d} γ* W-based sulfate Wells–Dawson cluster.[35]

Herein we describe the synthesis and structural characterization of the pure α and β forms of the clusters. Electrochemical data are reported in an acetonitrile and in anionic liquid and emphasize the formation of their one- and two-electron-reduced ions. Comparisons are made with the α-sulfate analogue and the α- and γ-$[W_{18}O_{54}(SO_4)_2]^{4-}$ isomers to assess the changes in redox properties introduced by replacement of sulfate by sulfite. EPR spectroscopy of the one-electron chemically reduced sulfite clusters at reduced temperatures (77 K) is able to distinguish between the two isomers. Further, we are able to deduce the extent of electron delocalization through the observation of spectral features due to the ^{95,97}Mo hyperfine interactions at liquid helium temperatures. Such observations appear to be without precedent in the EPR spectroscopy of the Mo_{18} Dawson–Wells type clusters. Finally, density functional theory (DFT) calculations are employed to help rationalize chemical and electronic properties.

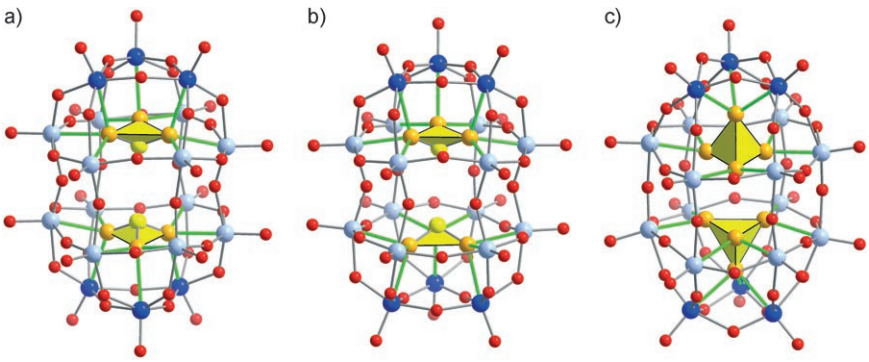

Figure 1. A ball-and-stick representation of the structures of the sulfite-based Dawson-like clusters: a) β-$[Mo_{18}O_{54}(SO_3)_2]^{4-}$ (**2a**), b) α-$[Mo^{VI}{}_{18}O_{54}(SO_3)_2]^{4-}$ (**1a**), and c) a comparison with the classical α-type sulfate-based Dawson anion $[Mo_{18}O_{54}(SO_4)_2]^{4-}$,[35] whereby the central anion templates are represented as yellow polyhedra. The bonds between the oxo positions of the heteroanions and the adjoined Mo positions are shown in green (S: yellow; O_{shell}: red; $O_{heteroanion}$: orange; capping Mo: dark blue; "belt" Mo: light blue).

Experimental Section

Synthesis: Crystalline samples of the molybdenum sulfite polyoxometalates were produced by adopting a solvent-mixture reaction previously reported[19] as follows: A solution of $Na_2MoO_4\cdot 2H_2O$ (4.8 g, 20 mmol) and Na_2SO_3 (0.45 g, 3.6 mmol) in H_2O (30 mL) was added with HCl 37% (9 mL), followed by the addition of

acetonitrile (50 mL). The resulting mixture was refluxed for 1 h and upon cooling, the mixture was added with tetrapentylammonium bromide (Pn_4NBr) (2.7 g) in water (600 mL) to afford a yellow precipitate and this was collected, washed with water, and dried under vacuum. Recrystallization of the solid in acetonitrile afforded firstly fine block orange crystals (yellow powder after losing solvated solvent) of $(Pn_4N)_4\{\beta\text{-}[Mo_{18}O_{54}(SO_3)_2]\}\cdot CH_3CN$ (**2**; yield 0.16 g, 3.6%), and then long lath orange crystals of $(Pn_4N)_4\{\alpha\text{-}[Mo_{18}O_{54}(SO_3)_2]\}\cdot CH_3CN$ (**1**; 0.96 g, 22%) and pale yellow crystals of $(Pn_4N)_2[Mo_6O_{19}]$ as the remaining by-product, which were separated mechanically. Although the α- and β-polyoxometalate anions found in **1** and **2** form in the same reaction system, experiments showed that they can be separated by recrystallization. For **1**, IR (KBr disk): $\tilde{\nu}=3448, 2956, 2870, 1480, 1379, 971, 902, 781\ cm^{-1}$; elemental analysis calcd (%) for $C_{80}H_{176}Mo_{18}N_4O_{60}S_2$ (losing solvent CH_3CN): C 24.35, H 4.50, N 1.42; found: C 24.38, H 4.40, N 1.49. For **2**, IR (KBr disk): $\tilde{\nu}=3436, 2956, 2870, 1481, 1380, 1246, 968, 903, 787\ cm^{-1}$; elemental analysis calcd (%) for $C_{80}H_{176}Mo_{18}N_4O_{60}S_2$ (losing solvent CH_3CN): C 24.35, H 4.50, N 1.42; found: C 24.32, H 4.32, N 1.37.

Electrochemical studies: Acetonitrile (Merck) containing the electrolytes Hx_4NClO_4 or Bu_4NPF_6 (Fluka of Puriss Grade) was used for all voltammetric studies in an organic solvent. Ionic liquid electrochemical studies were conducted in $BMIM\cdot PF_6$ (1-butyl-3-methylimidazolium hexafluorophosphate, >97%, Sigma-Aldrich), which was dried and purified over basic alumina before use. Solutions used for electrochemical studies were degassed with nitrogen for at least 10 min to remove dioxygen.

Electrochemical experiments were undertaken at (18±2)°C with a BAS 100 A Electrochemical Workstation (Bioanalytical Systems, West Lafayette, IN) using a standard three-electrode configuration. The working electrodes used for cyclic voltammetry were glassy carbon (1.5 mm diameter, Cypress Systems) or Pt (1 mm diameter) disks. The auxiliary electrode was a 1-mm diameter Pt wire. The quasi-reference electrode consisted of a silver wire dipped into CH_3CN (electrolyte) or in ionic liquid but separated from the test solution by a porous frit. The potential of the quasi-reference electrode was calibrated against that of the IUPAC-recommended Fc^+/Fc process (oxidation of Fc (Ferrocene) as an internal reference). Rotating-disc electrode experiments used a GC disc-electrode (3 mm diameter, Metrohm), which was rotated by a variable speed rotator (Metrohm 628–10).

The bulk electrolysis method was used to prepare the one- and two-electron-reduced species in acetonitrile. The working electrode was a Pt gauze basket placed in a glass cylinder with a porous glass frit in the base, which was arranged symmetrically inside a Pt gauze basket (the auxiliary electrode). The reference electrode was the same as used for cyclic voltammetry in acetonitrile. The auxiliary electrode compartment was filled with CH_3CN (0.1 M Hx_4NClO_4), while the working electrode compartment was filled with CH_3CN (0.1 M Hx_4NClO_4) containing α- or $\beta\text{-}[Mo_{18}O_{54}(SO_3)_2]^{4-}$. During bulk electrolysis, the working electrode was held at the appropriate potential and the solution was stirred vigorously. The electrolysis was stopped when the current achieved a value of 1% of the initial current. One- and two-electron-reduced compounds were isolated as solids by adding ethanol to electrolyzed solutions. The precipitate formed was collected by filtration and washed with ethanol. Dissolution back into acetonitrile, followed by slow diffusion of ethanol led to formation of microcrystalline material (not suitable for structural characterization by X-ray analysis).

The procedure for mechanical adherence of solid-state compounds onto the electrode surface is described in detail elsewhere.[37] In summary, a small amount of microcrystalline solid was placed on weighing paper, then the solid is adhered to the working electrode by pressing the surface onto the paper. The modified electrode was then directly placed in contact with the solvent (electrolyte) or ionic liquid solution. Prior to each electrochemical experiment, the working electrode was polished with a 0.05-μm Al_2O_3 (Buehler) slurry, washed with water, and dried with tissue paper.

Spectroscopic and EPR studies: UV/Vis and near IR spectra were recorded in a 1-mm path length cell using a Cary 5 spectrophotometer controlled by a personal computer. EPR experiments were carried out with a Bruker ESP 380E FT/CW X-band EPR spectrometer using either a standard rectangular TE_{012} cavity or a Bruker ER 4118 dielectric resonator. With the rectangular cavity, the temperature of 77 K was obtained with a Bruker liquid nitrogen finger Dewar. A nitrogen gas flow insert Dewar was used for temperatures between about 106 K and room temperature (~295 K). At least five minutes was allowed for thermal equilibrium to be established. Temperatures between 2.3 K and about 175 K were achieved with the dielectric resonator inserted in an Oxford Instruments CF 935 cryostat. The temperature was calibrated again a germanium thermometer using a carbon resistor as a transfer standard.

Microwave frequencies were measured with an EIP Microwave 548 A frequency counter and g values were determined with reference to the F^+ line in CaO ($g=2.0001\pm0.0002$).[38] EPR spectral simulations were performed by using the SOPHE software described by Hanson et al.[39] The SOPHE program takes account of the relative abundances of the various Mo nuclei. Benzyl alcohol (BDH) was added to an acetonitrile solution containing α- or $\beta\text{-}[Mo_{18}O_{54}(SO_3)_2]^{4-}$ and the samples were exposed to sunlight in a soda glass container to assess the photoactivity of these sulfite polyoxometalates.

Theoretical studies: Density functional theory (DFT) calculations were carried out using the TURBOMOLE 5.7 package employing B3-LYP functionals and TZV(P) basis sets including effective core potentials for Mo. All systems were allowed to relax geometrically until the total energy remained consistent within $10^{-3}\ kJ\,mol^{-1}$, whereby maximal position shifts of <0.15 Å were observed (most pronounced for terminal oxo centers).[40]

X-ray crystallographic studies: Suitable single crystals of **1** and **2** were selected from the crystallization and were mounted on a thin glass fiber using Fomblin oil. X-ray intensity data were measured at 150(2) K on a Nonius Kappa-CCD diffractometer [$\lambda(Mo_{K\alpha})=0.71073$ Å]. Data were processed by using Denzo and Sortav or EvalCCD software. Structure solution and refinement for **1** and **2** were carried out with SHELXS-97 and SHELXL-97 by using WinGX.[41] Empirical absorption corrections for incident and diffracted beam absorption effects were applied. Both structures were solved by a combination of direct methods and difference Fourier syntheses and refined against F^2 by the full-matrix least-squares technique. The Mo atoms were initially located by direct methods, and all other non-H atoms were found by successive difference Fourier syntheses. Only molybdenum and oxygen atoms were refined anisotropically. Owing to high thermal disorder in the Pn_4N^+ ion positions, these were only approximately refined by utilizing suitable restraints of the N–C and C–C distances. However, although the crystallographic analysis does result in relatively high R values as a result of this disorder, this does not affect the interpretation of the cluster geometries. Indeed, both the α and β isomers are well defined. As in **1**, there are two $\alpha\text{-}[Mo_{18}O_{54}(SO_3)_2]^{4-}$ clusters in the asymmetric unit, both with D_{3h} symmetry, and the two sulfite groups are eclipsed. In **2**, only half of the $\beta\text{-}[Mo_{18}O_{54}(SO_3)_2]^{4-}$ cluster is defined by an asymmetric unit, the other half being related by an inversion center, which confirms the cluster has D_{3d} symmetry; as expected for the β isomer. Crystal data, data collection parameters and refinement statistics for **1** and **2** are listed in Table 1.

CCDC-279456 (**1**) and CCDC-279457 (**2**) and contain the supplementary crystallographic data (excluding structure factors) for structures in this paper. These data can be obtained free of charge from the Cambridge Crystallographic Data Centre via www.ccdc.cam.ac.uk/data_request/cif.

Results and Discussion

Syntheses: In our previous work,[29] the synthesis and separation of α and β isomers of sulfite-based polyoxometalate $\{Mo_{18}\}$ clusters using tetrabutylammonium as crystallization cations was reported. However, using this approach, the α isomer always co-crystallizes with a Lindqvist anion $[Mo^{VI}{}_6O_{19}]^{2-}$ and this is not optimal for the measurement of the electrochemical properties. Therefore other cations of variable size including Pn_4N^+, tetrapropylammonium

Table 1. Crystallographic data for compounds **1** and **2**.

	1	**2**
empirical formula	$C_{80}H_{176}Mo_{18}N_4O_{60}S_2$	$C_{80}H_{176}Mo_{18}N_4O_{60}S_2$
M_r [g mol^{-1}]	3945.3	3945.3
crystal system	monoclinic	monoclinic
a [Å]	58.4432(9)	18.8881(5)
b [Å]	18.0521(3)	18.8034(4)
c [Å]	26.4620(4)	20.2033(5)
β [°]	94.399(1)	96.825(1)
space group	$P2_1/c$	$P2_1/n$
V [Å^3]	27844.6(6)	7124.6(3)
Z	8	2
ρ_{calcd} [g cm^{-3}]	1.902	1.858
μ [cm^{-1}]	1.672	1.633
T [K]	150(2)	150(2)
no. observations	36915	6004
residuals[a]: R; R_w	0.0672; 0.184	0.080; 0.278

[a] $R1 = \Sigma\,||F_o| - |F_c||/\Sigma\,|F_o|$. $wR2 = \{\Sigma[w(F_o^2 - F_c^2)^2]/\Sigma[w(F_o^2)^2]\}^{1/2}$.

(Pr_4N^+), tetrahexaylammonium (Hx_4N^+), and tetraphenylphosphonuim (Ph_4P^+) were examined. The products with Ph_4P^+ and Pr_4N^+ ions are sparingly soluble in acetonitrile and no products are obtained using Hx_4N^+, with only $[Mo^{VI}{}_6O_{19}]^{2-}$ salts being isolated. However Pn_4N^+ is found to be ideal and it was possible to successfully separate the two isomers avoiding co-crystallization of other polyanions. Further, it was also found that the same polyoxometalate product exists in the aqueous layer from the original synthesis and can be recovered by treating both layers with Pn_4NBr. This significantly increased the yield for the β isomer. It appears the α isomer has much higher solubility than the β isomer. In addition, the re-crystallizations, if not disturbed, yield very large crystals (mm) of $[Mo^{VI}{}_6O_{19}]^{2-}$ salts as a by-product, which can be separated mechanically. The β isomer forms first as fine orange crystal blocks (size ~0.2 mm), and the α isomer only crystallizes out when the solution is nearly at dryness, producing long brown lath-shaped crystals (up to many mm in length).

Structural analysis of compounds 1 and 2: Compound **1** crystallizes as a monoclinic system with two α-$[Mo_{18}O_{54}(SO_3)_2]^{4-}$ (**1a**) anions and eight Pn_4N^+ ions found in the asymmetric unit, plus some positions that can be identified as disordered solvent (CH_3CN). Cluster **1a** incorporates two pyramidal sulfite SO_3^{2-} ions as the central cluster templates and displays an overall approximate D_{3h} symmetry, with the horizontal plane dividing the cage into two equal parts linked together by six equatorial oxo ligands, see Figure 1a. Unlike conventional Dawson clusters, **1a** shows the distinctive peanut-like shape of the $\{Mo_{18}O_{54}\}$ framework. Similar structures have also been observed for $\{W_{18}O_{54}\}$-type cages in the non-conventional Dawson-type compounds $(Me_4N)_6[W_{18}O_{54}(OH)_3(BiO_3)]$[23] and $(H_4N)_7[W_{18}O_{54}(O)(OH)_2(AsO_3)]$.[24] Notably, **1a** is almost isostructural to 18-molybdopyrophosphate $[Mo_{18}O_{54}(P_2O_7)]^{4-}$, which was previously reported in $(Bu_4N)_4[Mo_{18}O_{54}(P_2O_7)]$,[25–28] except in this latter case an oxo ligand connects the two phosphorus centers. The coordination mode for the template XO_3 in our clusters is significantly different from that of XO_4 in conventional Dawson forms. In conventional Dawson clusters, one of the four oxo ligands of the tetrahedral XO_4 moiety coordinates to the three capping M centers and the remaining three μ_3-oxo ligands each bridge two of the six "belt" M centers, see Figure 1. In both the Dawson and our clusters, the six "belt" M centers can be divided into three groups of two adjacent metal centers according to their environment with regards to the capping M centers, that is, two "belt" M centers with one capping M center forming a "closed triangle". In the coordination mode of a XO_4 heteroanion, three μ_2-oxo ligands can either bridge two "belt" M centers within one group or between groups, and this allows more isomers for conventional Dawson clusters, which total six in this μ_3-oxo case. However, in **1a** the μ_3-oxo ligands of an SO_3 moiety each individually bridge three molybdenum centers, one from the cap and two from the "belt". As such, it appears the oxo ligands on XO_3 can only bridge two "belt" M centers within the group of the "closed triangle". This fundamental difference between the XO_4 and XO_3 coordination modes restricts the possible isomers of the sulfite-based $\{Mo_{18}\}$ clusters to only the α and β types.[29]

Compound **2** crystallizes in the triclinic system with half the β-$[Mo_{18}O_{54}(SO_3)_2]^{4-}$ (**2a**) ions and two Pn_4N^+ ions found in the asymmetric unit plus one position for disordered solvent CH_3CN molecules. The other half of the β-$[Mo_{18}O_{54}(SO_3)_2]^{4-}$ is related by a center of symmetry. The whole cluster **2a** also incorporates two pyramidal sulfite SO_3^{2-} ions as the central cluster templates and displays an overall approximate D_{3d} symmetry, with a reflection center at the cluster center. Therefore the two sulfite SO_3^{2-} ions are centrosymmetrically related in a staggered conformation (see Figure 1).

To summarize, the D_{3h}-symmetric α (**1a**) and the D_{3d}-symmetric β (**2a**) type of the sulfite-based $\{Mo_{18}\}$ clusters are distinguished both by their metal–oxide framework and by the relative orientation of the two SO_3 moieties that are eclipsed in the α type (related by a mirror plane) and staggered in the β type (related centrosymmetrically). In addition to the arrangement of the anions in the cages, the α and β isomers also differ by the relative linkage of the two $\{SMo_9\}$ half units that are either mirrored (α) or rotated by 60° to each other (β).

Electrochemical studies in acetonitrile: *Cyclic voltammetry of α-$[Mo_{18}O_{54}(SO_3)_2]^{4-}$ in acetonitrile (0.1 M Hx_4NClO_4):* Voltammetric studies in the absence and presence of a range of supporting electrolytes (see Supporting Information) demonstrated that 0.1 M Hx_4NClO_4 was an ideal electrolyte because it enabled the necessary level of compound solubility to be retained in acetonitrile. The cyclic voltammetry for reduction of α-$[Mo_{18}O_{54}(SO_3)_2]^{4-}$ (1.18 mM) at a GC electrode in CH_3CN (0.1 M Hx_4NClO_4) is shown at a function of scan rate in Figure 2a when the potential is reversed after the third process. The first two processes (**I** and **II**) are well-defined, with the onset of complexity only commencing with the third process (**III**). Voltammograms obtained over a

wider potential range also exhibit significant complexity (Figure 2b) in the negative potential range, but basically consist of six chemically reversible processes when mM concentrations are employed (**I** to **VI**). No voltammetric oxidation of α-$[Mo_{18}O_{54}(SO_3)_2]^{4-}$ is observed. Processes **I** and **II** are ideal diffusion-controlled one-electron processes over the concentration (0.2 to 2 mM) and scan rate (20 to 2000 $mV\,s^{-1}$) ranges studied. This is evidenced by the linear dependence of peak height on concentration and square root of scan rate. Reversible potentials ($E_f°$) of −0.005 V and −0.265 V versus Fc^+/Fc (Table 2) are calculated from the average of the reduction (E_p^{red}) and oxidation (E_p^{ox}) peaks potentials. At a concentration of 0.276 mM and a scan rate of 20 $mV\,s^{-1}$, the peak-to peak separation ($\Delta E_p = E_p^{red} - E_p^{ox}$) for the first two processes are (0.071 ± 0.01) and (0.065 ± 0.01) V, essentially the same values found for the known reversible one-electron oxidation of ferrocene (used as an internal standard in these studies). Thus, the small departure from the ideal ΔE_p value of about 55 mV for a reversible process is attributed to a small level of uncompensated resistance. Equations (1) and (2) therefore represent the first two reduction processes:

$$\alpha\text{-}[Mo_{18}O_{54}(SO_3)_2]^{4-} + e^- \rightleftharpoons \alpha\text{-}[Mo_{18}O_{54}(SO_3)_2]^{5-} \quad (1)$$

$$\alpha\text{-}[Mo_{18}O_{54}(SO_3)_2]^{5-} + e^- \rightleftharpoons \alpha\text{-}[Mo_{18}O_{54}(SO_3)_2]^{6-} \quad (2)$$

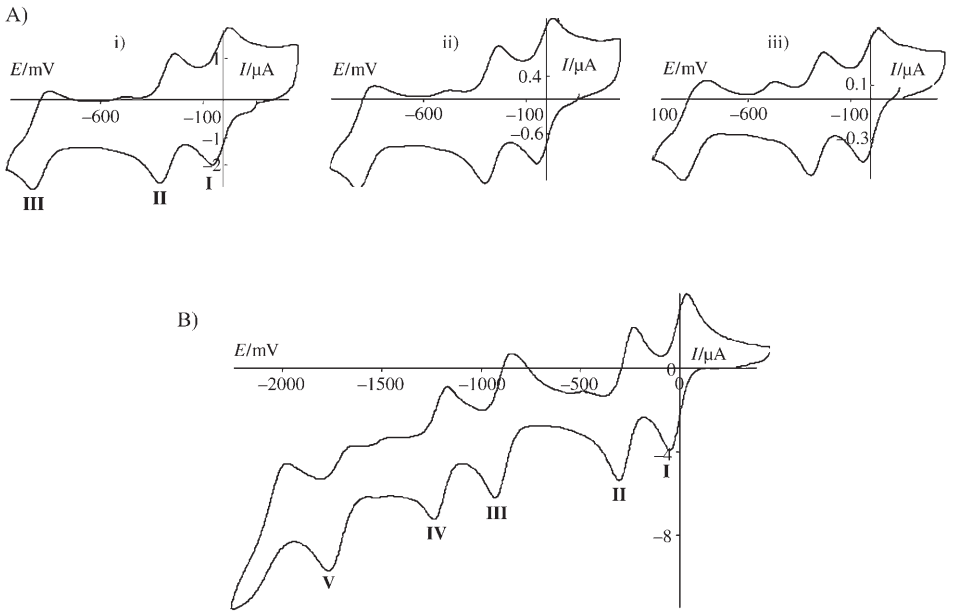

Figure 2. Cyclic voltammograms at a GC electrode (d = 1.5 mm) obtained for α-$[Mo_{18}O_{54}(SO_3)_2]^{4-}$ in CH_3CN (0.1 M Hx_4NClO_4): A) at a concentration of 0.276 mM (i) v = 200 $mV\,s^{-1}$, (ii) v = 100 $mV\,s^{-1}$ and (iii) v = 20 $mV\,s^{-1}$, and B) at a concentration of 1.18 mM, v = 20 $mV\,s^{-1}$. The vertical scale is I [μA] and the horizontal scale is E_0 [mV].

The voltammetric data described above do not allow the isomeric form of the reduced species to be assigned; however, EPR data (see below) indicate that retention of isomeric form accompanies the electron transfer processes given in Equations (1) and (2).

Process **III** detected at a potential near −0.9 V is broader than processes **I** and **II**. Both the shape and peak potential depend on the scan rate. Thus, ΔE_p for process **III** is 0.130 V at a scan rate of 200 $mV\,s^{-1}$ and 0.165 mV at a scan rate of 10 $mV\,s^{-1}$. Significantly, E_p^{ox} shifts to more positive values as the scan rate decreases (Figure 2a), and a new process is detected between processes **II** and **III** when the potential is swept in the positive potential direction. All these data are consistent with an electron-transfer process (E) followed by a coupled chemical reaction (C) in a so-called EC reaction process summarized by Equation (3):

$$\alpha\text{-}[Mo_{18}O_{54}(SO_3)_2]^{6-} + e^- \overset{E}{\rightleftharpoons} [Mo_{18}O_{54}(SO_3)_2]^{7-} \overset{C}{\rightleftharpoons} \text{product(s)} \quad (3)$$

It was established that the influence of the coupled chemical reaction is diminished when the concentration of α-$[Mo_{18}O_{54}(SO_3)_2]^{4-}$ is increased. Furthermore, the process on the reverse scan between processes **III** and **II** decreases when the scan rate increases, whereas the magnitude increases when acid is deliberately added. Consequently, the complexity associated with the third reduction process is attributed to the reaction of $[Mo_{18}O_{54}(SO_3)_2]^{7-}$ with protons derived from adventitious water [Eq. (4)] or other impurities.

$$[Mo_{18}O_{54}(SO_3)_2]^{7-} + H^+ \rightarrow [HMo_{18}O_{54}(SO_3)_2]^{6-} \quad (4)$$

Table 2. $E_f°$ values obtained at a GC electrode for the reduction of β-$[Mo_{18}O_{54}(SO_3)_2]^{4-}$ and α-$[Mo_{18}O_{54}(SO_3)_2]^{4-}$ in CH_3CN (0.1 M Hx_4NClO_4), at a scan rate of 20 $mV\,s^{-1}$, and for the reduction of α-$[Mo_{18}O_{54}(SO_4)_2]^{4-}$ in CH_3CN (0.1 M Bu_4NClO_4), at a scan rate of 100 $mV\,s^{-1}$.[35]

Processes	$E_f°$ in V versus Fc^+/Fc		
	β-$[Mo_{18}O_{54}(SO_3)_2]^{4-}$	α-$[Mo_{18}O_{54}(SO_3)_2]^{4-}$	$[Mo_{18}O_{54}(SO_4)_2]^{4-}$
I (**I′**)	−0.030	−0.005	0.100
II (**II′**)	−0.310	−0.265	−0.140
III (**III′**)	−0.880	−0.885	−0.800
IV (**IV′**)	−1.180	−1.195	−1.070
V (**V′**)	−1.660	−1.695	−1.670
VI (**VI′**)	−2.030	−2.075	−1.920

The more negative processes (**IV** to **VI**) are even less well defined at low $[Mo_{18}O_{54}(SO_3)_2]^{4-}$ concentrations. Since in principle the $[Mo_{18}O_{54}(SO_3)_2]^{8-/9-/10-}$ species generated in these reactions are even more basic, increased sensitivity to adventitious water is expected as the extent of reduction is increased. However, for $[Mo_{18}O_{54}(SO_3)_2]^{4-}$ concentrations in excess of 1 mM (Figure 2b), all processes exhibit significant chemical reversibility, when a sufficiently fast scan rate is employed, and data obtained under these conditions are summarized in Table 2.

Cyclic voltammetry of β-$[Mo_{18}O_{54}(SO_3)_2]^{4-}$ in acetonitrile (0.1 M Hx_4NClO_4): The β-$[Mo_{18}O_{54}(SO_3)_2]^{4-}$ isomer exhibits similar cyclic voltammetric behavior to that of the α-form. Thus, the two first processes (**I′** and **II′**) give $E_f°$ values of −0.030 ($\Delta E_p = 0.069$ V) and −0.310 V ($\Delta E_p = 0.065$ V), respectively (Figure 3). The shape of process **III′** ($E_f° = -0.880$ V) again depends on the scan rate and ΔE_p (0.130 V

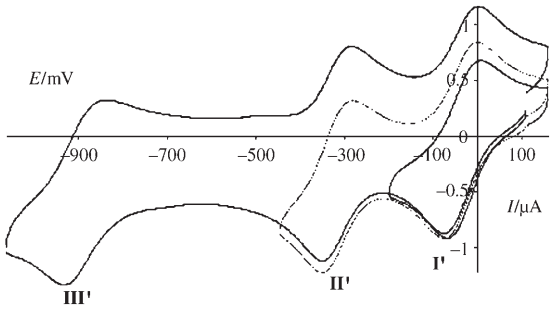

Figure 3. Cyclic voltammograms at a GC electrode ($d = 1.5$ mm) obtained for 0.242 mM β-$[Mo_{18}O_{54}(SO_3)_2]^{4-}$ in CH_3CN (0.1 M Hx_4NClO_4), $v = 20\,mV\,s^{-1}$ when the potential of scan reversal occurs at −0.193 V, −0.434 V, −1.050 V versus Fc^+/Fc. The vertical scale is I [μA] and the horizontal scale is E_0 [mV].

at a scan rate of $200\,mV\,s^{-1}$ and 0.170 mV at $10\,mV\,s^{-1}$). The current magnitude of the process present on the reverse scan between processes **III′** and **II′** is smaller than for the α isomer. These data are consistent with the presence of a kinetically slower coupled chemical reaction(s) than for the α isomer. As for the α isomer, six chemically reversible processes are again detected when mM concentrations of β-$[Mo_{18}O_{54}(SO_3)_2]^{4-}$ are employed, and data obtained from these experiments are summarized in Table 2.

Rotating disk electrode voltammetry: Reduction of α- and β-$[Mo_{18}O_{54}(SO_3)_2]^{4-}$ at a rotating GC disc electrode (RDE) gives rise to three well-defined sigmoidal shaped (Figure 4a) processes (**I′**), (**II′**) and (**III′**), with equal limiting current values (Table S1 in Supporting Information) even at lower concentrations (Figure 4a). $E_{1/2}$ values for the three processes are very similar to $E_f°$ values obtained by cyclic voltammetry as expected for the reaction sequence in Equation (5) being fully reversible under RDE conditions.

$$\beta\text{-}[Mo_{18}O_{54}(SO_3)_2]^{4-} + e^- \rightleftharpoons \beta\text{-}[Mo_{18}O_{54}(SO_3)_2]^{5-} \qquad (5)$$

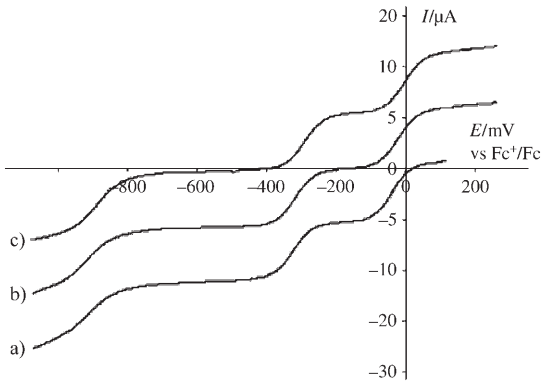

Figure 4. GC rotating disc-electrode ($d = 3$ mm) voltammograms obtained for 0.242 mM β-$[Mo_{18}O_{54}(SO_3)_2]^{4-}$ in CH_3CN (0.1 M Hx_4NClO_4), $v = 10\,mV\,s^{-1}$, $\omega = 1000$ rpm. a) Before electrolysis; b) after exhaustive one-electron reductive electrolysis at −0.200 V; c) after exhaustive two-electron reductive electrolysis at −0.500 V. The vertical scale is I [μA] and the horizontal scale is E_0 [mV].

Electronic spectra of α- and β-$[Mo_{18}O_{54}(SO_3)_2]^{4-}$: Electronic spectra of the α and β-isomers (Figure 5a) are similar. Absorption occurs over the wavelength range of 250–450 nm

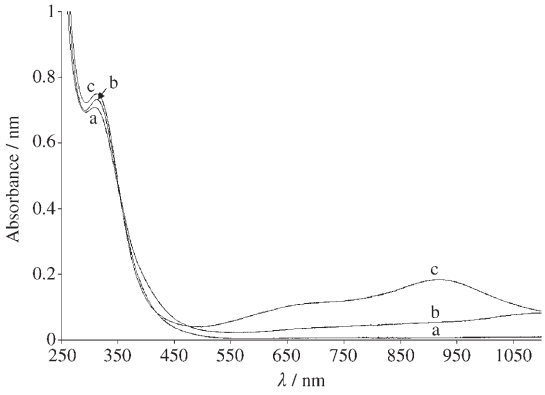

Figure 5. Electronic spectra obtained from 0.242 mM β-$[Mo_{18}O_{54}(SO_3)_2]^{4-}$ in CH_3CN (0.1 M Hx_4NClO_4), in a 1-mm cell: a) prior to electrolysis; b) after exhaustive one-electron reduction at −0.205 V; c) after exhaustive two-electron reduction at −0.485 V.

with λ_{max} at 301 nm ($\varepsilon = 30\,800\,M^{-1}cm^{-1}$) for the α isomer and 308 nm ($\varepsilon = 29\,250\,M^{-1}cm^{-1}$) for the β-isomer. The electronic spectra are characteristic of O→Mo charge transfer transitions.[43] Similar $E_f°$ data for the α-$[Mo_{18}O_{54}(SO_3)_2]^{4-/5-}$ and β-$[Mo_{18}O_{54}(SO_3)_2]^{4-/5-}$ processes correlates with similar λ_{max} values for their electronic spectra.

Controlled potential electrolysis: Controlled-potential electrolysis, combined with coulometry and monitoring of steady-state voltammograms during the course of bulk electrolysis (Figure 4) confirmed that the first two processes involve one-electron charge transition processes, even on these longer time scale experiments. Thus, exhaustive reduction of a 0.2 mM solution of $[Mo_{18}O_{54}(SO_3)_2]^{4-}$ in CH_3CN (0.1 M Hx_4NClO_4) at −0.200 V versus Fc^+/Fc led to a stable

solution of $[Mo_{18}O_{54}(SO_3)_2]^{5-}$ since steady-state voltammograms (Figure 4b) now consist of one oxidation process **I** (**I′**) and two reduction processes **II** (**II′**) and **III** (**III′**), with the position of zero current lying between processes **I** (**I′**) and **II** (**II′**). Furthermore, coulometric analysis confirms that a one-electron per molecule charge transfer process is associated with the $[Mo_{18}O_{54}(SO_3)_2]^{4-/5-}$ process for both isomers, and the initially yellow solution changes to a green color after a one-electron reduction. Electronic spectra from the one-electron-reduced solution still contain the charge transfer band around 300 nm, but with an increase of intensity (Figure 5b). Additionally, a new weak absorption band is observed in the near infrared region, which is a characteristic of intervalence $Mo^{V} \rightarrow Mo^{VI}$ charge transfer.[44]

More extensive reduction of $[Mo_{18}O_{54}(SO_3)_2]^{5-}$ at -0.500 V leads to a stable solution of $[Mo_{18}O_{54}(SO_3)_2]^{6-}$ as indicated by coulometry (one-electron reduction) and the fact that steady-state and cyclic voltammograms now consist of two oxidation processes **I** (**I′**) and **II** (**II′**) and one reduction process **III** (**III′**). Importantly, the position of zero current lies between process **II** (**II′**) and **III** (**III′**), as expected for two-electron reduced species (Figure 4c). During this electrolysis, the solution color changes from green to blue. Electronic spectra reveal that the absorption intensity of the $O \rightarrow Mo$ charge transfer band further increases, and the weak absorption band in the near infrared region shifts to the visible range, with a band at 914 nm ($\varepsilon = 7600$ and $8770\,M^{-1}cm^{-1}$ for the β- and α isomers, respectively) and a shoulder at 690 nm (Figure 5c). $[Mo_{18}O_{54}(SO_3)_2]^{6-}$ and $[Mo_{18}O_{54}(SO_3)_2]^{5-}$ may be quantitatively oxidized back to $[Mo_{18}O_{54}(SO_3)_2]^{4-}$, confirming the chemical reversibility of the $[Mo_{18}O_{54}(SO_3)_2]^{4-/5-}$ and $[Mo_{18}O_{54}(SO_3)_2]^{5-/6-}$ processes on the time scale of bulk electrolysis.

Bulk electrolysis of $[Mo_{18}O_{54}(SO_3)_2]^{6-}$ at -1.075 V does not produce a stable $[Mo_{18}O_{54}(SO_3)_2]^{7-}$ species by a one-electron reduction process. Rather a multielectron transfer process occurs, according to coulometric analysis, and complicated RDE voltammograms are obtained after reduction at this negative potential. This result is consistent with the complexity of the cyclic voltammetry associated with process **III**. Thus, we now focus on the isolable and stable one- and two-electron reduced species in the remainder of the paper.

Isolation of reduced solids: The one- and two-electron electrochemically reduced forms of the two isomers have been isolated as solids. Addition of ethanol to concentrated bulk electrolyzed solutions allowed separation of the electrolyte (Hx_4NClO_4 is soluble in ethanol, but the reduced forms of the compound are insoluble). The EPR spectra of the one-electron-reduced solids at 77 K are very similar to those of the one-electron-reduced species in an acetonitrile glass (see below). Unfortunately, the crystals were not of suitable quality for structural analysis.

Voltammetric studies with $(Bu_4N)_4$ β-$[Mo_{18}O_{54}(SO_3)_2]$: $(Bu_4N)_4[Mo_{18}O_{54}(SO_3)_2]CH_3CN$ has been isolated as the β-sulfite Dawson isomer.[29] However, it is insoluble in acetonitrile (electrolyte) media. Voltammetric studies of this compound, as a solid adhered to a glassy carbon electrode dipped in CH_3CN (0.1 M Hx_4NClO_4), produced results analogous to those found for soluble β-$[Mo_{18}O_{54}(SO_3)_2]^{4-}$ (as the $(Pr_4N)_4[Mo_{18}O_{54}(SO_3)_2]$ salt) in the same medium. In this case (Figure 6), three well-defined reversible processes are

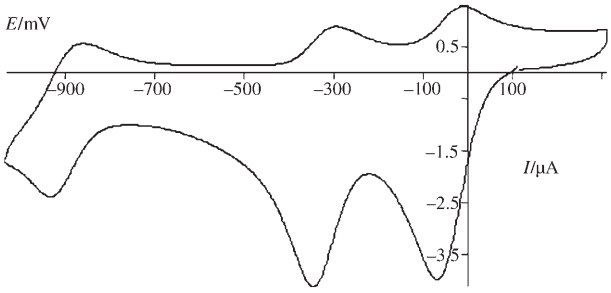

Figure 6. Cyclic voltammograms at a GC electrode ($d = 1.5$ mm) obtained for $(C_{16}H_{36}N)_4[Mo_{18}O_{54}(SO_3)_2]CH_3CN$ as a solid adhered to a glassy carbon electrode dipped in CH_3CN (0.1 M Hx_4NClO_4), $v = 100\,mV\,s^{-1}$.

again visible with E_f° values of -0.035, -0.320, and -0.900 V versus Fc^+/Fc. The nature of these voltammetric results imply that a rapid dissolution of the one-electron reduced solid occurs as in Equation (6).

$$(Bu_4N)_4\{\beta\text{-}[Mo_{18}O_{54}(SO_3)_2]\}_{(solid)} + e^- + (Hx_4N)^+ \rightarrow (Bu_4N)_4(Hx_4N)\{\beta\text{-}[Mo_{18}O_{54}(SO_3)_2]\}_{(solid)} \xrightarrow{fast} \{\beta\text{-}[Mo_{18}O_{54}(SO_3)_2]^{5-}\}_{(solution)} + 4\,(Bu_4N^+)_{(solution)} + (Hx_4N^+)_{(solution)} \quad (6)$$

Voltammetry in BMIM·PF_6: Cyclic voltammograms were recorded for α- and β-$[Mo_{18}O_{54}(SO_3)_2]^{4-}$ dissolved in the ionic liquid BMIM·PF_6 and also for solid adhered to a glassy carbon electrode in contact with the ionic liquid. In both cases, three very well-defined one-electron-reduction processes are readily detected with E_f° values of 0.325, 0.202, and -0.208 versus Fc^+/Fc for the α isomer and 0.310, 0.175 and -0.260 V for the β isomer (Figure S2, Table S2 in the Supporting Information). Again additional, but more complex reduction processes are found at more negative potentials, but not considered in further detail. The potentials obtained in the ionic liquid follow the same order as in acetonitrile (0.1 M Hx_4NClO_4), but occur at significantly more positive values versus Fc^+/Fc. These observations imply that the trends are not altered by the change in medium, but that the high polarity of the ionic liquid has a significant influence on the absolute value of E°_f, as also reported in studies of other polyoxometalate species.[45]

EPR spectroscopy: Both the α and β isomers of the one-electron-reduced product gave strong EPR signals in frozen acetonitrile solution as described below. Frozen acetonitrile solutions of the two-electron-reduced products gave only weak signals (due to trace levels of the one-electron prod-

uct) when examined at high spectrometer gains and over a field range from zero to 6000 G. Both isomers were deduced to retain their configuration upon one- and two-electron reduction in acetonitrile (0.1 M Hx_4NClO_4) by noting that a two-electron reduction (formation of $[Mo_{18}O_{54}(SO_3)_2]^{6-}$), followed by a one-electron oxidation (formation of $[Mo_{18}O_{54}(SO_3)_2]^{5-}$) sequence provides EPR spectra identical to those observed from a direct one-electron reduction of the relevant α- or β-$[Mo_{18}O_{54}(SO_3)_2]^{4-}$ isomer.

X-band EPR spectra of one-electron reduced $[Mo_{18}O_{54}(SO_3)_2]^{5-}$: Both isomers showed a single featureless, isotropic resonance at $g=1.940$ (± 0.002), which decreased in width from (75 ± 2) G at 295 K to (58 ± 1) G at 200 K. Below about 170 K the spectra gradually became more axially symmetric in appearance (see Figure S3 in the Supporting Information). Below about 130 K the spectra of the two isomers differ and show that no interconversion occurs in frozen solution. Further resolution into spectra with the appearance of orthorhombic symmetry was exhibited by the α isomer below about 120 K and by the β isomer below 77 K. At temperatures around 4 K and below and at microwave powers below about 1 μW, the spectra of the two isomers are readily distinguished, as shown in Figure 7 and Figure 8. The sharp

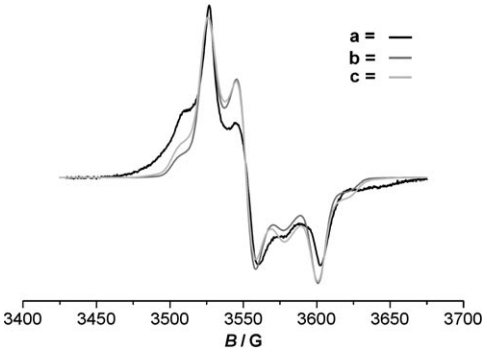

Figure 7. a) Experimental EPR spectrum of millimolar frozen solutions (in CH_3CN, 0.1 M Hx_4NClO_4) of α-$[Mo_{18}O_{54}(SO_3)_2]^{5-}$ at 2.3 K. Microwave frequency 9.666 GHz, microwave power 209 nW, 100 kHz modulation amplitude 1 G, spectrometer gain 1.0×10^4, time constant 41 ms, scan rate 250 G/83 s. b) Simulated EPR spectrum for two-molybdenum cluster, and c) simulated EPR spectrum for three-molybdenum cluster, using spin Hamiltonian parameters as in Table 3.

peaks with g values given in Table 3 are attributed to even isotope (nuclear spin $I=0$) Mo ions in sites of orthorhombic symmetry. These g values are typical for Mo^V with the unpaired electron in the $4d^1$ ground state. The z direction is taken as being in the direction of the oxygen heteroanions and approximately perpendicular to the surface of the cluster, with the x and y directions being associated with the approximate plane of the "shell" oxygen atoms. The expected six-line Mo hyperfine patterns with spacings of ($\sim$30–80)$\times10^{-4}$ cm^{-1}[46,47] are not observed. Together with the temperature dependence of the spectra, this shows that the unpaired electron density is distributed over a number of Mo sites.

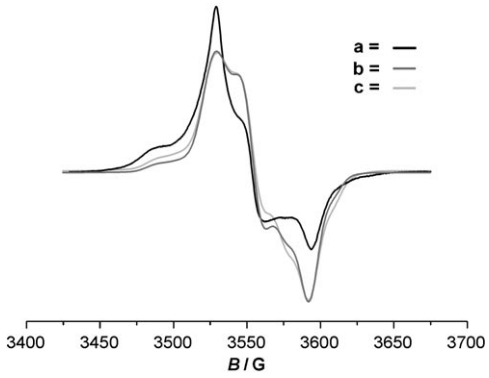

Figure 8. a) Experimental EPR spectrum of millimolar frozen solutions (in CH_3CN, 0.1 M Hx_4NClO_4) of β-$[Mo_{18}O_{54}(SO_3)_2]^{5-}$ at 2.3 K. Microwave frequency 9.655 GHz, microwave power 209 nW, 100 kHz modulation amplitude 1 G, spectrometer gain 1.0×10^4, time constant 41 ms, scan rate 250G/83 s. b) Simulated spectrum for two-molybdenum cluster, and c) simulated spectrum for three-molybdenum cluster, using spin Hamiltonian parameters as in Table 3.

Table 3. The g values and hyperfine interaction constants for α-$[Mo_{18}O_{54}(SO_3)_2]^{5-}$ and β-$[Mo_{18}O_{54}(SO_3)_2]^{5-}$ at 2.3 K in CH_3CN. The hyperfine interaction, A, and the component linewidths, σ, are in units of 10^{-4} cm^{-1}. Note the uncertainties for the g values for the β isomer are larger than those for the α isomer because of the larger line widths in the former and the x and y hyperfine features for the β isomer were not as well defined in the experimental spectrum as the corresponding features for the α isomer. The values of A_x and A_y have a larger uncertainty than A_z.

	α isomer			β isomer		
	g ($\pm$0.0003)	A ($\pm$0.5)	σ ($\pm$0.5)	g ($\pm$0.001)	A	σ ($\pm$1)
x	1.9175	8.0	5.0	1.920	6($\pm$2)	6
y	1.9440	7.5	5.0	1.941	6($\pm$2)	7
z	1.9585	7.5	5.0	1.956	14($\pm$1)	8

The deviation of the g values from g_e is due to spin-orbit coupling and is essentially independent of electron delocalization since the spin-orbit interaction only operates on the electronic component of the wave functions. As the Mo coordination environment is very similar for both isomers, it is unsurprising that the g values are almost identical. The component linewidths of the spectrum of clusters, for which all Mo nuclei have $I=0$, are determined solely by relaxation effects and not by the unresolved hyperfine structure.

When the unpaired electron is delocalized over n Mo sites, the EPR spectrum is the superposition of the $n+1$ spectra from clusters for which the number of Mo nuclei with nuclear spin $I=5/2$ ranges from zero to n. As described in the Supporting Information, the relative abundance of these clusters can be calculated by using the binomial theorem and the isotopic abundances of the Mo nuclei (^{95}Mo 15.9%, ^{97}Mo 9.6% both $I=5/2$: ^{92,94,96,98,100} Mo 74.5%, all $I=0$. For the present purposes we ignore the difference in nuclear moment between ^{95}Mo and ^{97}Mo). The overall width of the spectrum of a cluster for which p nuclei have $I=5/2$ increases as $2I\cdot pA$, where A is the relevant hyperfine interaction. As shown in the Supporting Information, the most prominent features of the spectrum will be those due to clusters containing only Mo nuclei with $I=0$ and the next

most prominent those where only one of Mo Nuclei of the cluster has $I=5/2$. Furthermore, since computer simulation shows that "flat-topped" shoulder features can only arise when there is one $I=5/2$ nucleus involved and when the hyperfine splitting is of a similar magnitude to the linewidth, we identify the shoulders at about 3505 G (α isomer), at about 3485 G (β isomer) and the features at around 3575 and 3625 G (α isomer) and 3575 and 3605 G (β isomer) as due to clusters with only one $I=5/2$ nucleus. If the cluster includes two or more $I=5/2$ nuclei, the line shape assumes a Gaussian appearance. Contributions from clusters with two or more $I=5/2$ nuclei presumably account for the broad tails to both low and high fields and some of the spectral intensity in the central regions of the 2.3-K spectra.

Unfortunately computer limitations prevented us from simulating spectra where delocalization occurs over more than three Mo sites. Furthermore, the simulation model makes a first-order approximation by assuming that the g and A axes of the individual Mo sites are coincident and coparallel for each Mo nucleus in the cluster. Simulated spectra for delocalization over two and three Mo ions are compared with the experimental spectra of the α isomer in Figure 7 and the β isomer in Figure 8. The spin-Hamiltonian parameters are listed in Table 3. The simulations account well for the g values, for the magnitudes of the hyperfine interactions in the "z" directions, but not as satisfactorily for the hyperfine interactions in the "x" and "y" directions and the relative intensities of the various regions of the spectra.

Despite the limitations of the computer simulations, an estimate of the number of Mo ions over which the unpaired electron is delocalized can be obtained as described in the Supporting Information. A comparison of the intensity of the g_z resonance of the α isomer with that of the outermost A_z hyperfine structure resonance in the shoulder feature at 3505 G gives a factor of approximately three and thus we deduce that the unpaired electron is delocalized over six Mo sites. For the β isomer, the intensity of the g_z resonance may be estimated as being between five and eight times that of the outermost A_z hyperfine structure resonance at about 3485 G, leading to the conclusion that the unpaired electron is delocalized over an average of three Mo sites. Symmetry and structural considerations lead us to propose that at very low temperatures, the unpaired electron density is localized on one cap region in the β isomer and over both cap regions, with quantum-mechanical tunneling between them, in the α isomer, rather than over part of the belt region.

Irrespective of the limitations of the computer modeling, it is necessary to account for the temperature dependence of the spectra, the nearly isotropic Mo hyperfine structure for the α complex, the axial Mo hyperfine structure for the β complex and the occurrence of orthorhombic g-matrices for both complexes. The latter is perhaps surprising given the likely threefold symmetry of the complexes as shown by X-ray structural determinations at 150 K. We suggest the following qualitative arguments to explain these observations.

The temperature dependences of the spectra are influenced by the rate of fluctuation of the electron density over the relevant Mo sites. This depends on the rate at which the local structure of the Mo sites distorts, the rate at which the unpaired electron hops between Mo sites, and the rate of quantum-mechanical tunneling between sites. The first two processes are temperature dependent, whereas the third is not. If any of these rates is greater than the difference between the energy of the relevant components of the g matrix or A tensor (expressed as a frequency) an average value will be observed. Conversely, if the rates are slower, anisotropic effects will be observed. The anisotropy between the components of the g matrix is about 100 MHz, whereas that between the components of the. hyperfine tensor, A, is only about 10 MHz.

For the β isomer, we can then explain the three g factors by the unpaired electron density being delocalized predominantly over three Mo sites on the cap with the individual g and A principal directions oriented essentially along and perpendicular to the molecular symmetry axis. As the temperature is lowered below about 77 K, the molecular distortion rate has slowed sufficiently for the unpaired electron density to be seen as centered slightly away from the expected molecular axis, allowing the components of the g matrix to be distinguished. There are three of these off-center sites which, assuming the z axis is along the expected molecular axis, are rotated by 120° with respect to each other. However, the unpaired electron density is still able to fluctuate between these sites sufficiently rapidly to average the hyperfine interaction in the xy plane so that $<A_{\perp}(\beta)>=\frac{1}{2}[A_x(\beta)+A_y(\beta)]$ but not rapidly enough in the z direction to include $A_z(\beta)$ in the averaging process. Thus the hopping rate between the three equivalent distortions must be lower than 100 MHz but greater than about 10 MHz.

For the α isomer, delocalization over six Mo sites suggests that the unpaired electron is delocalized equally over the two cap regions and undergoes quantum-mechanical tunneling between them, rather than being delocalized over part of the belt region. The three principal g factors are thought to occur in the same way as for the β isomer, except that the distortions are frozen in at around 120 K. However, in addition to the fluctuation between the three distortions on each cap, the tunnelling rate between the two caps introduces the fluctuation in the z direction necessary to include $A_z(\alpha)$ in the average, so that we obtain an isotropic Mo hyperfine structure where $<A_{iso}(\alpha)>=\frac{1}{3}[A_x(\alpha)+A_y(\alpha)+A_z(\alpha)]$.

As noted elsewhere in this paper, a feature of the present clusters is that the Mo^V-O-Mo^V bond angles linking the two Mo^V halves of the molecule in the belt region are around 142° rather than the approximately 180° found in the conventional "Dawson -like" clusters. The smaller bond angle will hinder transmission of electron density across the belt region and confine the electron density to the surface of one half of the cluster. Furthermore the 60° rotation of the sulfite oxygen atoms of the two groups relative to each other in the β isomer could present a barrier to electron transfer via quantum-mechanical tunneling between the cap regions. These considerations are consistent with our proposal that at low temperatures the unpaired electron is confined to a

single cap region in the β isomer but is able to tunnel via the sulfite groups between both cap regions in the α isomer.

Photoactivity: α- and β-$[Mo_{18}O_{54}(SO_3)_2]^{4-}$, as is the case with α-$[Mo_{18}O_{54}(SO_4)_2]^{4-}$,[48,49] exhibit photoactivity. Thus, solutions of both isomers in acetonitrile are reduced on exposure to sunlight in the presence of benzyl alcohol [Eq. (7)]. The initial formation of reduced $[Mo_{18}O_{54}(SO_3)_2]^{5-}$ was implied by observation of a change in the color of the solution from yellow to green and confirmed by detection of the EPR signal expected on the basis of earlier discussions.

$$[Mo_{18}O_{54}(SO_3)_2]^{4-} \xrightarrow{h\nu,\ \text{benzyl alcohol}} [Mo_{18}O_{54}(SO_3)_2]^{5-} + \text{oxidized benzyl alcohol} \quad (7)$$

On prolonged exposure to sunlight, more extensive conversion to the two-electron-reduced form of $[Mo_{18}O_{54}(SO_3)_2]^{6-}$ occurs, as confirmed by a change in the color of the solution from green to blue and by the decrease of the intensity of the EPR signal.

Long-term isomeric stability of reduced species in solution: The EPR spectra of electrochemically or photochemically generated acetonitrile solutions of α- and β-$[Mo_{18}O_{54}(SO_3)_2]^{5-}$ stored at room temperature in the dark or exposed each day to sunlight have been monitored for a period of 37 days. EPR spectra were obtained periodically at 77 K to identify the isomer present. Either in the light or in the dark, slow β-→α-$[Mo_{18}O_{54}(SO_3)_2]^{5-}$ isomerization occurs, whereas the reverse reaction α-→β-$[Mo_{18}O_{54}(SO_3)_2]^{5-}$ is not observed. Additionally, electrogenerated solutions of α- and β-$[Mo_{18}O_{54}(SO_3)_2]^{6-}$ stored in the dark for 30 days in acetonitrile (0.1 M Hx_4NClO_4) then electro-oxidized by one electron to produce the $[Mo_{18}O_{54}(SO_3)_2]^{5-}$ species also show that, β-→α-$[Mo_{18}O_{54}(SO_3)_2]^{6-}$ isomerization occurs, as deduced from EPR spectra at 77 K. These data imply that α-$[Mo_{18}O_{54}(SO_3)_2]^{5-}$ and α-$[Mo_{18}O_{54}(SO_3)_2]^{6-}$ rather than the β-forms are the thermodynamically favored reduced forms and that isomerization of β-$[Mo_{18}O_{54}(SO_3)_2]^{5-}$ is not facilitated by the presence of sunlight nor by photo-induced reduction of $[Mo_{18}O_{54}(SO_3)_2]^{4-}$ in the presence of benzyl alcohol.

Comparison of electrochemical data with $[Mo_{18}O_{54}(SO_4)_2]^{4-}$ and other polyoxometalates: Six primary chemically reversible one-electron-reduction processes appear to be available for reduction of the both α- and β-$[Mo_{18}O_{54}(SO_3)_2]^{4-}$ in acetonitrile (0.1 M Hx_4NClO_4) according to the reaction scheme in Equation (8).

$$\begin{aligned}&[Mo_{18}O_{54}(SO_3)_2]^{4-} + e^- \rightleftharpoons [Mo_{18}O_{54}(SO_3)_2]^{5-} + e^- \rightleftharpoons\\ &[Mo_{18}O_{54}(SO_3)_2]^{6-} + e^- \rightleftharpoons [Mo_{18}O_{54}(SO_3)_2]^{7-} + e^- \rightleftharpoons\\ &[Mo_{18}O_{54}(SO_3)_2]^{8-} + e^- \rightleftharpoons [Mo_{18}O_{54}(SO_3)_2]^{9-} + e^- \rightleftharpoons\\ &[Mo_{18}O_{54}(SO_3)_2]^{10-}\end{aligned} \quad (8)$$

In the case of reduction of α-$[Mo_{18}O_{54}(SO_4)_2]^{4-}$ in acetonitrile (0.1 M Bu_4NClO_4), at least six one-electron-reduction processes also may be obtained.[20,35,37b] Data for the first six processes for all the sulfite and the sulfate compounds of interest are included in Table 2. In the sulfate polyoxometalate case, pairs of reduction processes spaced by about 260 mV, each separated by a gap in excess of 580 mV, is the characteristic pattern.[35] In the case of the sulfite Dawson, reduction is considerably more difficult (about 100 mV more negative in potential) but a similar pattern of behavior is detected. In this case, three pairs of one-electron processes exhibit a separation of about 300 mV, which increases with the extent of the reduction, whereas a larger potential gap in excess of 500 mV is detected between each of the pairs, with this gap decreasing with the extent of reduction.

The reversible potentials also may be compared to those reported for $[M_{18}O_{54}(XO_4)_2]^{6-}$ (X = P, As; M = Mo, W) in aqueous sulfate solution.[50,51] For this series, the tungsten compounds also show six successive one-electron processes as three pairs, when the pH value is sufficiently high. Under these conditions their difference in potential within each pair is about 200 mV, and the separation between pairs lies in the range between 250 mV and 600 mV. $[Mo_{18}O_{54}(PO_4)_2]^{6-}$ is more easily reduced than its tungsten analogue but only three successive two-electron processes are observed in aqueous media. That is attributed to its reduced anions being much stronger bases than their tungsten analogues, and they become protonated in aqueous media. Data obtained from cyclic voltammetry also reveals a propensity for protonation of extensively reduced forms of $[Mo_{18}O_{54}(SO_3)_2]^{4-}$. However, the one-electron-reduced species $[Mo_{18}O_{54}(SO_3)_2]^{5-}$ is stable to disproportionation, as are its sulfate analogue[35] and $[P_2Mo_{18}O_{62}]^{7-}$, under aprotic conditions.[52]

Only an α isomer has been isolated for the $[Mo_{18}O_{54}(SO_4)_2]^{4-}$ species, so the dependence of the reversible potential on the isomeric form is unknown for this polyoxometalate. However, in the case of $[W_{18}O_{54}(SO_4)_2]^{4-}$, reversible potentials for the α and γ* forms are indistinguishable,[35] and the γ*→α conversion appears to occur on reduction.[35] In the $[Mo_{18}O_{54}(SO_3)_2]^{4-}$ case, two isomers were characterized and the reversible potentials for the $[Mo_{18}O_{54}(SO_3)_2]^{4-/5-}$ process exhibit very small differences (between 10 and 30 mV). As noted in the Introduction, the D_{3d}-symmetric β isomer in the sulfite case may be reasonably compared in a symmetry sense with the γ* (D_{3d}) sulfate isomer, and this seems to be borne out by the redox properties and the nature of the isomerization detected upon reduction. Studies on $[M_{18}O_{54}XO_4]^{y-}$ (M = Mo, W; α = P, As) systems, in which the number of isomers are far more extensive than for the sulfite case, reveal that reversible potentials are generally not strongly dependent on the isomeric form and that isomeric stability and the orders of reversible potential are delicately balanced.[35,45,51–54]

Theoretical studies: Immediately upon one- and two-electron electrochemical reduction, EPR experiments show that both isomers of $[Mo_{18}O_{54}(SO_3)_2]^{5-}$ species retain their configuration. However, β→α isomerization occurs very slowly

with time, implying that the α form is the thermodynamically favored structure in the reduced states.

To gain insight whether stability relations similar to those observed in the electrochemical experiments can also be expected for the isolated, non-solvated cluster species, closed-shell ab initio DFT calculations were performed on the α and β isomer in their fully oxidized and twofold reduced states in the gas phase. We find that the DFT results indeed support the experimental results. While the total energies of the oxidized α and β isomers of $[Mo_{18}O_{54}(SO_3)_2]^{4-}$ are identical within the error limits of the used methods, the twofold reduced α-$[Mo_{18}O_{54}(SO_3)_2]^{6-}$ isomer is significantly more (7.4 kJ mol^{-1}) stable than the two-fold reduced β isomer, which supports the fact that the observed β→α isomerization is based on thermodynamic differences. Likewise, these differences suggest that a two-electron reduction of the α isomer should be energetically more favorable than a two-electron reduction of the β isomer.

Conclusion

Voltammetric and bulk electrolysis experiments in acetonitrile, combined with EPR data, have shown that α- and β-$[Mo_{18}O_{54}(SO_3)_2]^{4-}$ as well as their one- (α- and β-$[Mo_{18}O_{54}(SO_3)_2]^{5-}$) and two-electron-reduced (α- and β-$[Mo_{18}O_{54}(SO_3)_2]^{6-}$) isomers are stable over the time scale of electrochemical studies. Over a long period of time in solution (about 30 days) β→α isomerization is detected for the one- and two-electron-reduced species. EPR data imply that the unpaired electron in $[Mo_{18}O_{54}(SO_3)_2]^{5-}$ is localized on caps sites at very low temperature, in an isomer-dependent manner; in the α-$[Mo_{18}O_{54}(SO_3)_2]^{5-}$ isomer the unpaired electron is localized on both cap sites, whereas it is localized on only one cap site in the β-$[Mo_{18}O_{54}(SO_3)_2]^{5-}$ isomer. However, we do not have enough information to decide whether the appearance of the spectra at higher temperatures is due to the averaging effects of vibrational and rotational motions alone or to the combination of these with increased electron delocalization.

More highly reduced polyoxometalate species have been observed on the voltammetric time scale, but they are highly reactive towards water, protons and probably dioxygen. α-$[Mo_{18}O_{54}(SO_3)_2]^{4-}$ is significantly harder to reduce than α-$[Mo_{18}O_{54}(SO_4)_2]^{4-}$, but also is photoactive and exhibits many similar electrochemical patterns of behavior. The reversible potentials for α and β isomers are very similar, with the β isomer being marginally harder to reduce in acetonitrile (0.1 M Hx_4NClO_4) and also in the ionic liquid BMIM·PF_6. DFT-based theoretical calculations, relevant to the gas phase, are consistent with the assignment of the enhanced stability of the α isomer relative to the β form upon reduction, as deduced experimentally in solution-phase studies.

Acknowledgements

The authors gratefully acknowledge financial support from the Leverhulme Trust (D.L. and L.C.), EPSRC (D.L. and L.C.), the Australian Research Council (C.B. and A.M.B.) and the School of Physics (J.F.B. and J.R.P.). Ames Laboratory is operated for the U.S. Department of Energy by Iowa State University, Contract No. W-7405-Eng-82.

[1] A. Müller, S. Roy, *Coord. Chem. Rev.* **2003**, *245*, 153.
[2] *Polyoxometalates—From Platonic Solids to Anti-Retroviral Activity*, (Eds.: M. T. Pope, A. Müller), Kluwer, Dordrecht, The Netherlands, **1994**, pp. 1–411.
[3] N. Mizuno, M. Misono, *Chem. Rev.* **1998**, *98*, 199–217.
[4] C. L. Hill, *Angew. Chem.* **2004**, *116*, 406–408; *Angew. Chem. Int. Ed.* **2004**, *43*, 402–404.
[5] C. L. Hill in *Comprehensive Coordination Chemistry II, Vol. 4*, (Eds.: J. A. McCleverty, T. J. Meyer), Elsevier, Amsterdam, **2004**, p. 679.
[6] K.-F. Aguey-Zinsou, P. V. Bernhardt, U. Kappler, A. G. McEwan, *J. Am. Chem. Soc.* **2003**, *125*, 530–535.
[7] D. A. Judd, J. H. Nettles, N. Nevins, J. P. Snyder, D. C. Liotta, J. Tang, J. Ermolieff, R. F. Schinazi, C. L. Hill, *J. Am. Chem. Soc.* **2001**, *123*, 886–897.
[8] B. Hasenknopf, *Front. Biosci.* **2005**, *10*, 275–287.
[9] H. Zeng, G. R. Newkome, C. L. Hill, *Angew. Chem.* **2000**, *113*, 1841–1844; *Angew. Chem. Int. Ed.* **2000**, *39*, 1771–1774.
[10] M. T. Pope, A. Müller, *Angew. Chem.* **1991**, *103*, 56–70; *Angew. Chem. Int. Ed. Engl.* **1991**, *30*, 34–48.
[11] F. Ogliaro, S. P. de Visser, S. Cohen, P. K. Sharma, S. Shaik, *J. Am. Chem. Soc.* **2002**, *124*, 2806–2817.
[12] T. R. Zhang, W. Feng, R. Lu, C. Y. Bao, T. J. Li, Y. Y. Zhao, J. N. Yao, *J. Solid State Chem.* **2002**, *166*, 259–263.
[13] T. Yamase, *Chem. Rev.* **1998**, *98*, 307–325.
[14] S. Liu, D. Volkmer, D. G. Kurth, *Anal. Chem.* **2004**, *76*, 4579–4582.
[15] B. Dawson, *Acta Crystallogr.* **1953**, *9*, 113–126.
[16] M. Holscher, U. Englert, B. Zibrowius, W. Holderich, *Angew. Chem.* **1994**, *106*, 2552–2554; *Angew. Chem. Int. Ed. Engl.* **1994**, *33*, 2491–2493.
[17] H. Ichida, Y. Sasaki, *Acta Crystallogr. Sect. C* **1983**, *39*, 529–533.
[18] R. Neier, C. Trojanowski, R. Mattes, *J. Chem. Soc. Dalton Trans.* **1995**, 2521–2528.
[19] P. J. S. Richardt, R. W. Gable, A. M. Bond, A. G. Wedd, *Inorg. Chem.* **2001**, *40*, 703–709.
[20] D. M. Way, J. B. Cooper, M. Sadek, T. Vu, P. J. Mahon, A. M. Bond, R. T. C. Brownlee, A. G. Wedd, *Inorg. Chem.* **1997**, *36*, 4227–4233.
[21] S. Zhu, B. Yue, X. Shi, Y. Gu, J. Liu, M. Chen, Y. Huang, *J. Chem. Soc. Dalton Trans.* **1993**, 3633–3634.
[22] F. H. Herbstein, R. E. Marsh, *Acta Crystallogr. Sect. B* **1998**, *54*, 677–686.
[23] Y. Ozawa, Y. Sasaki, *Chem. Lett.* **1987**, 923–926.
[24] Y. Jeannin, J. Martin-Frere, *Inorg. Chem.* **1979**, *18*, 3010–3014.
[25] T. Hori, M. Sugiyama, S. Himeno, *Chem. Lett.* **1988**, 1017–1020.
[26] S. Himeno, A. Saito, T. Hori, *Bull. Chem. Soc. Jpn.* **1990**, *63*, 1602–1606.
[27] U. Kortz, M. T. Pope, *Inorg. Chem.* **1994**, *33*, 5643–5646.
[28] U. Kortz, *Inorg. Chem.* **2000**, *39*, 623–624.
[29] D.-L. Long, P. Kogerler, L. Cronin, *Angew. Chem.* **2004**, *116*, 1853–1856; *Angew. Chem. Int. Ed.* **2004**, *43*, 1817–1820.
[30] K. Y. Matsumoto, M. Kato, Y. Sasaki, *Bull. Chem. Soc. Jpn.* **1976**, *49*, 106–110.
[31] M. J. Manos, J. D. Woollins, A. M. Z. Slawin, T. A. Kabanos, *Angew. Chem.* **2002**, *114*, 2928–2929; *Angew. Chem. Int. Ed.* **2002**, *41*, 2801–2805.
[32] R. Hille, *Chem. Rev.* **1996**, *96*, 2757–2816.
[33] R. Hille, *J. Biol. Inorg. Chem.* **1997**, *2*, 804–809.
[34] A. V. Astashkin, A. M. Raitsimring, C. Feng, J. L. Johnson, K. V. Rajagopalan, J. H. Enemark, *J. Am. Chem. Soc.* **2002**, *124*, 6109–6118.

[35] P. J. S. Richardt, J. M. White, P. A. Tregloan, A. M. Bond, A. G. Wedd, *Can. J. Chem.* **2001**, *79*, 613–620; R. Contant, R. Thouvenot, *Inorg. Chim. Acta* **1993**, *212*, 41–50; J. Zhang, A. M. Bond, P. J. S. Richardt, A. G. Wedd, *Inorg. Chem.* **2004**, *43*, 8263–8271; S. Himeno, H. Tatenaki, M. Hashimoto, *Bull. Chem. Soc. Japan* **2001**, *74*, 1623.

[36] D. M. Way, A. M. Bond, A. G. Wedd, *Inorg. Chem.* **1997**, *36*, 2826–2833.

[37] a) F. Scholz, B. Meyer, *Electroanal. Chem.* **1998**, *20*, 1–86; b) A. M. Bond, *Broadening Electrochemical Horizons*, Oxford University Press, Oxford, **2002**.

[38] J. E. Wertz, J. W. Orton, P. Auzins, *Discuss. Faraday Soc.* **1961**, *31*, 140–150.

[39] G. R. Hanson, K. E. Gates, C. J. Noble, M. Griffin, A. Mitchell, S. Benson, *J. Inorg. Biochem.* **2004**, *98*, 903–916. [Monash University is a beta-testing site for the SOPHE software.)

[40] Density, functional theory calculations (including Löwdin and Mulliken population analysis) using the TURBOMOLE package (O. Treuler, R. Ahlrichs, *J. Chem. Phys.* **1995**, *102*, 346). For a recent review on ab initio calculations on POMs, see ref. [55].

[41] Anon, *J. Appl. Crystallogr.* **1999**, *32*, 837–838.

[42] A. M. Bond, *Trends in Molecular Electrochemistry*, FrontsMedia SA, Lausanne, **2004**, Chap. 14.

[43] G. M. Varga Jr., E. Papaconstantinou, M. T. Pope, *Inorg. Chem.* **1970**, *9*, 662–667.

[44] J. M. Fruchart, G. Herve, J. P. Launay, R. Massart, *J. Inorg. Nucl. Chem.* **1976**, *38*, 1627–1634.

[45] J. Zhang, A. M. Bond, D. R. MacFarlane, S. A. Forsyth, J. M. Pringle, A. W. A. Mariotti, A. F. Glowinski, A. G. Wedd, *Inorg. Chem.* **2005**, *44*, 5123–5132.

[46] a) C. Sanchez, J. Livage, J. P. Launay, M. Fournier, Y. Jeannin, *J. Am. Chem. Soc.* **1982**, *104*, 3194; b) T. Yamase, M. Suga, *J. Chem. Soc. Dalton Trans.* **1989**, 661; c) J. N. Barrows, M. T. Pope, *Inorg. Chim. Acta* **1993**, *213*, 91–98; d) P. T. Manoharan, M. T. Rogers, *J. Chem. Phys.* **1968**, *49*, 5510–5519; e) M. L. Scullane, R. D. Taylor, M. Minelli, J. T. Spence, K. Yamanouchi, J. H. Enemark, N. D. Chasteen, *Inorg. Chem.* **1979**, *18*, 3213–3219.

[47] A first-order crystal field calculation using the g values observed here gives hyperfine splittings with the tensor components being $A_x = 39$, $A_y = 36$, $A_z = 85 \times 10^{-4}\,\mathrm{cm}^{-1}$ see: G. L. Wilson, R. J. Greenwood, J. R. Pilbrow, J. T. Spence, A. G. Wedd, *J. Am. Chem. Soc.* **1991**, *113*, 6803–6812.

[48] T. Ruether, A. M. Bond, W. R. Jackson, *Green Chem.* **2003**, *5*, 364–366.

[49] T. Ruether, V. M. Hultgren, B. P. Timko, A. M. Bond, W. R. Jackson, A. G. Wedd, *J. Am. Chem. Soc.* **2003**, *125*, 10133–10143.

[50] E. Papaconstantinou, M. T. Pope, *Inorg. Chem.* **1967**, *6*, 1152–1155.

[51] M. T. Pope, E. Papaconstantinou, *Inorg. Chem.* **1967**, *6*, 1147–1152.

[52] J. N. Barrows, M. T. Pope, *Inorg. Chim. Acta* **1993**, *213*, 91–98.

[53] M. T. Pope, *Heteropoly and Isopoly Oxometalates*, Springer, New York, **1983**, Ch. 4.

[54] J. M. Poblet, X. Lopez, C. Bo, *Chem. Soc. Rev.* **2003**, *32*, 297–308.

[55] H. Duclusaud, S. A. Borshch, *J. Am. Chem. Soc.* **2001**, *123*, 2825–2829.

Received: November 22, 2005
Revised: April 14, 2006
Published online: September 5, 2006

